Phase-Separated CsI-NaCl Scintillator With Optical Guiding Function

Toru Den, Tatsuya Saito, Ryoko Horie, Yoshihiro Ohashi, and Nobuhiro Yasui

***Abstract*—We demonstrate a new scintillator material that has a one-dimensional eutectic structure and optical light-guiding properties. Our light propagation calculations predicted that a structure where high refractive index luminescence cylinders are embedded in a matrix should show effective light-guiding properties. An inverse structure where a high refractive index luminescence matrix contains low refractive index cylinders was also predicted to possess light-guiding properties. A CsI—NaCl:Tl eutectic phase, which contained NaCl cylinders in a CsI matrix, was grown by a one-dimensional solidification method. This material showed high spatial resolution because of the difference in the refractive indices of NaCl and CsI.**

***Index Terms*—Crystal microstructure, halides, scintillator, spatial resolution.**

I. Introduction

In current X-ray flat panel detectors, a $Gd_2O_2S:Tb$ (GOS) powder sheet or a CsI:Tl film is used as a scintillator [1], [2]. GOS has a high light yield and is relatively inexpensive. The CsI film is composed of needle-like CsI crystals which are oriented normal to the panel plane, and the light-guiding properties of the film arise from this characteristic structure. This structure means that the CsI film has high spatial resolution, even though the film is thicker than the GOS sheet. For future applications, such as next-generation mammography and X-ray phase contrast imaging, a higher resolution scintillator with high detective quantum efficiency (DQE) is required.

In this article, we propose a one-dimensional phase-separated scintillator (PSS) as an efficient light-guiding material candidate. One dimensional eutectic systems have been discovered for various materials [3]–[11]. Fig. 1 shows a schematic of its structure, which is composed of cylinders in a matrix. In the phase-separated $CaF_2 - MgO$ system, the MgO cylinders, which have high refractive index, can effectively guide the light flux from the back to the front surface in total reflection mode, because of the optically smooth side boundaries [3]. A characteristic length of phase separations is in the μm range when eutectic phases are made through a melt-solidification process and it becomes in the nm range when they are made through a vapor-phase growth process [10], [11]. Although numerous studies have been published in this eutectic material field, most of them have been related to solder materials and high-strength ceramics. The goals of this study are to show the dependence of light-guiding efficiency on refractive indices by calculations and also show an alkali halide phase-separated material system with scintillation functions and demonstrate its X-ray imaging capability.

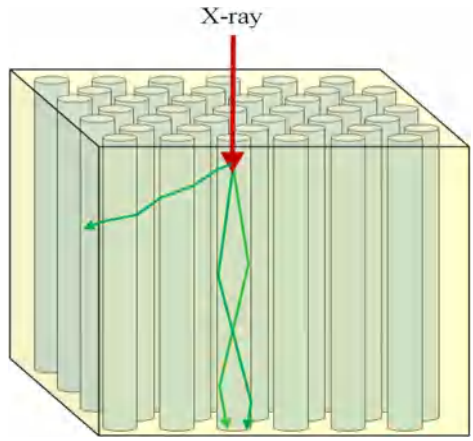

Fig. 1. Schematic of the PSS. The luminescent light is confined by the critical incident angle and propagates downward to a photodetector plane at the bottom in total reflection mode.

II. Calculations of Light Propagation

The flux collection efficiencies of the emitted light for various refractive indices of the cylinders and matrix were calculated using LightTools (Optical Research Associates). The calculation area was a 500 μm cube; the X-ray exposed area was a 50 μm square on the top surface, and the bottom surface was set as the photodetector layer. The emitted light for each calculation was 60,000 photons. In this calculation, the noise caused by cascades like Swank noise was left out of consideration to focus on the light propagation effect. The cylinders were arranged in a honeycomb geometry normal to the surface and were surrounded by the matrix in the cubic calculation area (see Fig. 1). The refractive index of the cylinders was n_c and that of the matrix was n_m, and the ratio (n_m/n_c) was varied from 0.575 to 2.0 (the ratio of the refractive indices of CsI and NaCl is about 1.15, more details about real parameters are provided later). The diameters of the cylinders were 4.6, 5.4, and 5.9 μm, and the distance between centers of the cylinders was 6.0 μm for all cases. The absorption coefficient was the same as that for 36 keV X-rays in CsI. The top surface was a mirror and the lateral sides were nonreflecting walls.

Manuscript received April 10, 2012; revised August 03, 2012 and November 27, 2012; accepted December 05, 2012. Date of publication January 30, 2013; date of current version February 06, 2013.

The authors are with Frontier Research Center, Canon Inc., 30-2-3 Shimomaruko, Ohta-ku, Tokyo 146-8501, Japan (e-mail: den.toru@canon.co.jp).

Color versions of one or more of the figures in this paper are available online at http://ieeexplore.ieee.org.

Digital Object Identifier 10.1109/TNS.2012.2233751

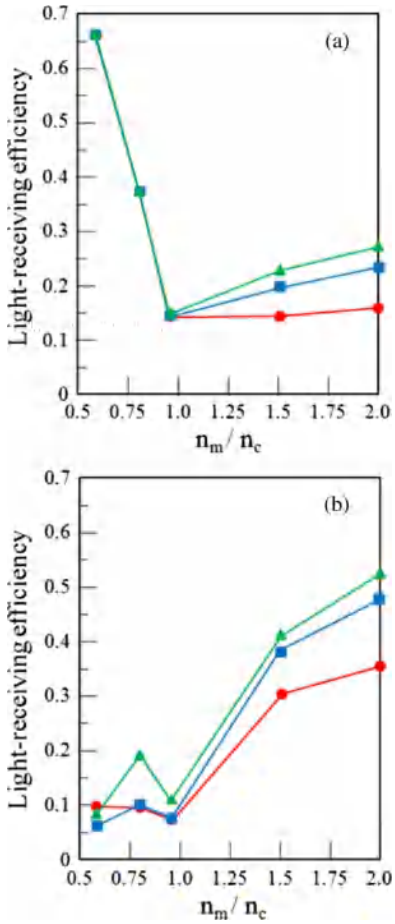

Fig. 2. The light receiving efficiencies depend on the ratio of the refractive index of the matrix to the refractive index of the cylinder (n_m/n_c). The relationship is shown for the cylindrical phase emission (Fig. 2(a)), and the matrix emission (Fig. 2(b)). In both graphs, the dependence on cylinder diameter is shown; 4.6 μm of diameter (closed circles), 5.4 μm (closed squares), and 5.9 μm (closed triangles). "Color figure online"

Fig. 2(a) and 2(b) show how the light-receiving efficiencies depend on the refractive index ratio (n_m/n_c), where the light-receiving efficiency is the ratio of the number of photons detected on the bottom surface just below the X-ray exposed area to the total number of emitted photons. Fig. 2(a) shows the emission of the cylinder phase, and demonstrates that the efficiency is superior when the ratio of n_m/n_c become small. This is analogous to an optical fiber or the needle-like CsI crystal films. The efficiency increases with the cylinder diameter as can be seen from the data of 4.6 μm of diameter (closed circles), 5.4 μm (closed squares), and 5.9 μm (closed triangles). Fig. 2(b) shows the inverse scenario; when the matrix emits light, the efficiency increases with the ratio n_m/n_c. Even when the matrix emits light, the efficiency can be increased when the ratio n_m/n_c and/or the cylinder volume fraction are large. When decreasing the ratio n_m/n_c from 1, the efficiency increases somewhat and then decreases with smaller ratios. This effect is because the emitted light from the matrix can enter waveguide mode when n_c becomes large relative to n_m, but as n_c becomes still larger, the emitted light tends to refract to the direction parallel to the bottom surface, and the amount of light that escapes to the sidewalls increases. As a result, the efficiency decreases again (the left side in Fig. 2(b)).

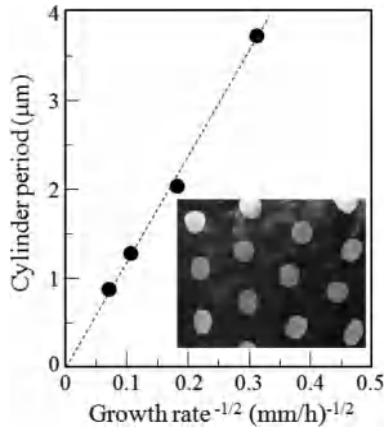

Fig. 3. The average period (λ) between the centers of the cylinders is controlled by the solidification speed (v), while satisfying the condition $v\lambda^2 = \text{constant}$. The inset picture shows the cross-sectional TEM image.

From these calculations, we can understand that the phase to be operated as the scintillator should have a higher refractive index relative to that of the other phase, and the ratio of the refractive index of scintillator phase to the refractive index of the other phase should be large to achieve better optical guiding properties. We have found out many phase separated scintillator materials [12] with eutectic compositions; among them we selected a CsI-NaCl phase system because the scintillator phase of CsI has a higher refractive index, and a cylinder phase of NaCl has rather large volume fraction. In this CsI-NaCl system, the CsI becomes the matrix phase and NaCl is the cylinder phase, so the volume fraction of a cylinder phase should be large to increase the light-receiving efficiency (see the closed-triangle-line in Fig. 2(b)).

III. Experimental Results

Some eutectic phases have an ordered structure, consisting of a cylindrical phase in a matrix, when they are grown by a one-dimensional solidification method [3], [4]. However, they do not scintillate. There are many low-melting-point alkali halides, which are practical scintillators; therefore we examined alkali halide systems. Some systems (CsI-NaCl, CsI-RbF, RbI-NaCl, CsBr-NaCl, CsBr-NaF, and RbCl-NaCl) formed a one-dimensional phase-separated structure which displayed scintillation properties [12]. The CsI—NaCl system had a well-aligned phase-separated structure, composed of NaCl cylinders and a CsI matrix. In this system, the eutectic point occurred where CsI = 70 mol% and NaCl = 30 mol%, and the eutectic temperature was 485°C. The inset of Fig. 3 shows the transmission electron microscopy (TEM) image of the top view of the CsI—NaCl:Tl sample, indicating that the NaCl cylinders had a diameter of 0.8 μm and a period of 1.8 μm. The diameter and period can be partly controlled by varying the solidification speed. Fig. 3 shows the dependence of the mean cylinder period (λ) on the solidification speed (v). The period varied from 1 to 4 μm when the solidification speed

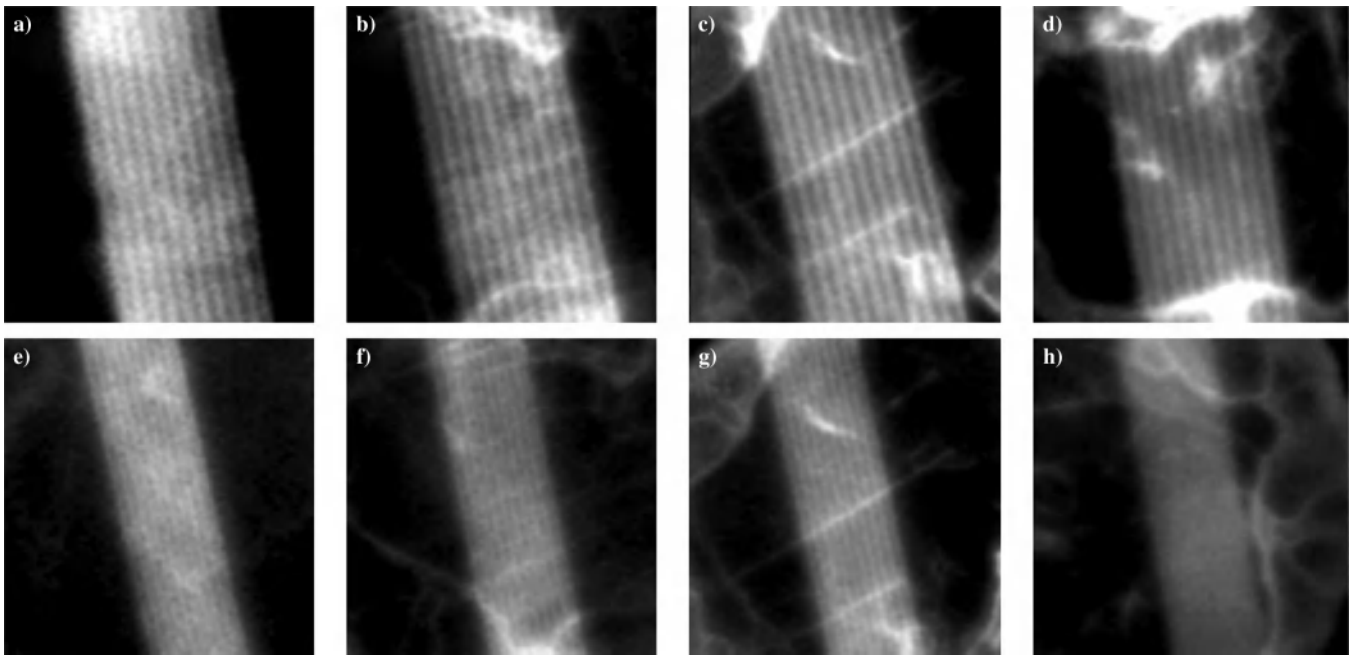

Fig. 4. The upper pictures (a)–(d) show the X-ray chart images for the 5 lp/mm pattern, and the bottom pictures (e)–(h) show images for the 8 lp/mm pattern. The images were taken with (a), (e) a 200-μm-thick PSS; (b), (f) a 420-μm-thick PSS; (c), (g) a 770-μm-thick PSS; and (d), (h) a 1.4-mm-thick PSS.

was changed from 230 mm/h to 10 mm/h, while satisfying the condition $v\lambda^2 = \text{constant}$ [13], where the constant depends on the material system.

The CsI matrix guided the light in total reflection mode, because the CsI refractive index $(\mathrm{n_m} = 1.78)$ is larger than that of NaCl $(\mathrm{n_c} = 1.55)$. The matrix was bright when the sample was illuminated from the back using an optical microscope. Only the luminescence from the CsI matrix was observed around 540 nm, under X-ray and UV irradiation.

Fig. 4 shows images taken using a Pb test chart (Pb thickness is 50 μm) with several line pair (lp) pattern widths, where the X-ray tube voltage was 60 $\mathrm{kV_p}$ and the current was 1 mA and the filter was Al plate of 3 mm thickness. Images were taken by the CCD via a lens optical-system (Nyquist limiting frequency is 10 lp/mm), and exposure time was about 6 seconds. The scintillators were set under the test chart, and the scintillator—the X-ray source distance was about 220 mm. In this figure, all PPS samples had cylinders with 1.6 μm diameter and a period of about 3.7 μm. The bulk PSS samples were grown by the one-dimensional solidification method described above. Thick samples were grown to varying thickness of a few cm, and cut perpendicular to the growth direction. After polishing the samples, the Al layer was deposited on the top surface as a reflecting coating. The upper figures are images of the 5 lp/mm pattern and the bottom figures are images of the 8 lp/mm pattern for a 200-μm-thick CsI—NaCl:Tl (a and e), a 420-μm-thick CsI—NaCl:Tl (b and f), a 770-μm-thick CsI—NaCl:Tl (c and g), and a 1.4-mm-thick CsI—NaCl:Tl (d and h). Some defects were visible in the images taken with the PSS scintillators, although the fine patterns can be clearly recognized with the PPSs. Fig. 4(g) indicates that the 8 lp/mm chart was recognizable even with the 770-μm-thick PPS. The contrast ratio obtained from the X-ray imaging data, which was calculated by the formula $(\mathrm{I_{max}} - \mathrm{I_{min}})/(\mathrm{I_{max}} + \mathrm{I_{min}})$, was ~4–6% for all of the PSS scintillators. The monotonic decrease of the contrast with the increase of the thickness was not confirmed because of the defects of the PPS samples. The average brightness of the PPS increases with the increase of the scintillator thickness from 200 μm to 1.4 mm.

The thickness of the PPS is easily increased by cutting from bulk samples, so the thickness can be designed so as to absorb X-ray adequately depending on X-ray energy.

IV. Conclusion

In summary, we have carried out light propagation calculations and showed dependences of the light-guiding efficiency of phase-separated structures on refractive indices of the phases, indicating that both the cylindrical and the matrix light-guiding structures can behave as scintillators with light-guiding properties. We also have demonstrated that the CsI—NaCl eutectic phase possesses light-guiding effects by imaging an X-ray test chart. The eutectic phase has a one-dimensional structure, where NaCl cylinders are arranged in a honeycomb geometry in a CsI matrix. PSSs will be grown in a similar manner to a crystal; therefore they can be grown as thick scintillator plates with the thickness adjustable to the X-ray energy. A long list of eutectic phases have been studied for various applications, so we believe that there are other eutectic scintillator materials to be found and PSSs will be a candidate for practical X-ray imaging scintillators.

References

[1] T. Yamazaki, T. Tamura, M. Nokita, S. Okada, S. Hayashida, and Y. Ogawa, "Performance of a novel 43-cm × 43-cm flat-panel detector with CsI:Tl scintillator," *Proc. SPIE*, vol. 5368, no. 379, 2004.

[2] C. W. E. van Eijk, "Inorganic scintillators in medical imaging," *Phys. Med. Biol.*, vol. 47, pp. R85–R106, 2002.

[3] A. Larrea, L. Contreras, R. I. Merino, J. LLorca, and V. M. Orera, "Microstructure and physical properties of $CaF_2 - MgO$ eutectics produced by the Bridgman method," *J. Mater. Res.*, vol. 15, pp. 1314–1319, 2000.

[4] J. LLorca and V. M. Orera, "Directionally solidified eutectic ceramic oxides," *Prog. Mater. Sci.*, vol. 51, pp. 711–809, 2006.

[5] H. Bei and E. P. George, "Microstructures and mechanical properties of a directionally solidified NiAl—Mo eutectic alloy," *Acta Mater.*, vol. 53, pp. 69–77, 2005.

[6] K. Kolodziejak, S. Turczynski, R. Diduszko, L. Klimek, and D. A. Pawlak, " $Tb_3Sc_2Al_3O_{12} - TbScO_3$ eutectic self-organized microstructure for metamaterials and photonic crystals application," *Opto-Electron. Rev.*, vol. 14, pp. 205–211, 2006.

[7] Y. Paderno, V. Paderno, N. Shitsevalova, and V. Filippov, "The peculiarities of the structure formation in directionally crystallized eutectics $EuB_6 - MeB_2$," *J. Alloys Compd.*, vol. 317, pp. 367–371, 2001.

[8] L. Mohaddes-Ardacili, H. Zheng, S. B. Ogale, B. Hannoyer, W. Tian, and J. Wang *et al.*, "Self-assembled single-crystal ferromagnetic iron nanowires formed by decomposition," *Nat. Mater.*, vol. 3, pp. 533–538, 2004.

[9] H. Zheng, J. Wang, S. E. Lofland, Z. Ma, L. Mohadded-Ardabili, and T. Zhao *et al.*, "Multiferroic $BaTiO_3 - CoFe_2O_4$ nanostructures," *Science*, vol. 303, pp. 661–663, 2004.

[10] K. Fukutani, K. Tanji, T. Motoi, and T. Den, "Ultrahigh pore density nanoporous films produced by the phase separation of eutectic Al—Si for template-assisted growth of nanowire array," *Adv. Mater.*, vol. 16, pp. 1456–1460, 2004.

[11] N. Yasui, R. Horie, Y. Ohashi, K. Tanji, and T. Den, "Well-aligned nanocylinder formation in phase-separated metal-silicide-silicon and metal-germanide-germanium systems," *Adv. Mater.*, vol. 19, pp. 2797–2801, 2007.

[12] N. Yasui, Y. Ohashi, T. Kobayashi, and T. Den*.*, , (to be published in Advanced Materials), to be published.

[13] A. W. Hassel, B. Bello-Rodriguez, S. Milenkovic, and A. Schneider, "Electrochemical production of nanopore arrays in a nickel aluminium alloy," *Electrochim. Acta*, vol. 50, pp. 3033–3039, 2005.